Supplemental Information

Structure and functional characterization of the RNA-binding element of the NLRX1 innate immune receptor

Minsun Hong, Sung-il Yoon and Ian A. Wilson

Inventory of Supplemental Figures

Figure S1, related to Figure 1

Figure S2, related to Figures 1-5

Figure S3, related to Figure 4

Figure S4, related to Figures 5

Figure S5, related to Figure 1

A

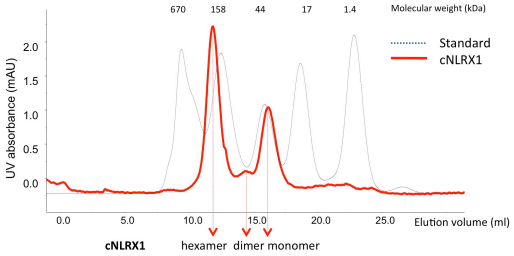

B

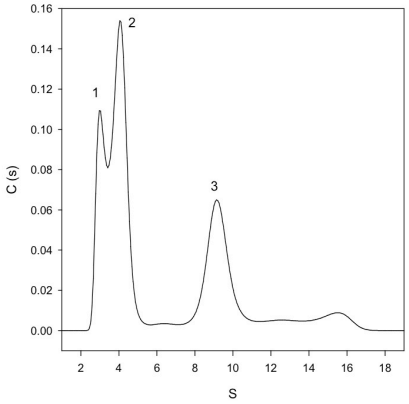

Peak no.	Percent (%)	App. Mw (kDa)	Estimated Mw (kDa)	
1	18.2	43.6	40.5	monomer
2	35.8	66.7	81.0	dimer
3	23.6	227.5	243.0	hexamer

C

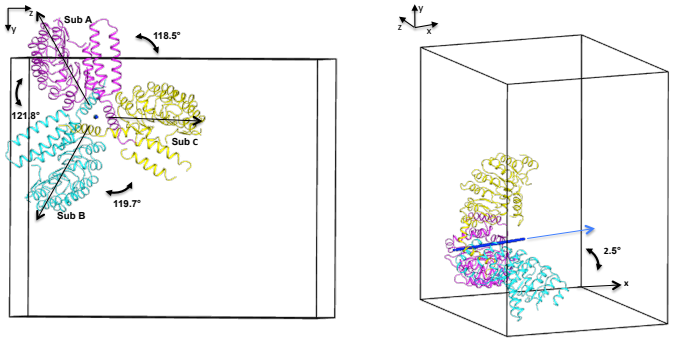

D

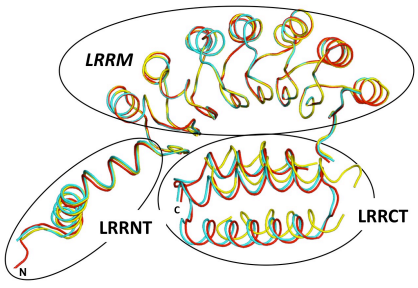

r.m.s.d. (Å)	All^{A}	LRRNT^{A}	LRRM^{A}	LRRCT^{A}	All^{B}	LRRNT^{B}	LRRM^{B}	LRRCT^{B}
B	0.5	0.1	0.1	0.2				
C	1.0	0.1	0.1	2.1	1.1	0.1	0.1	2.2

E

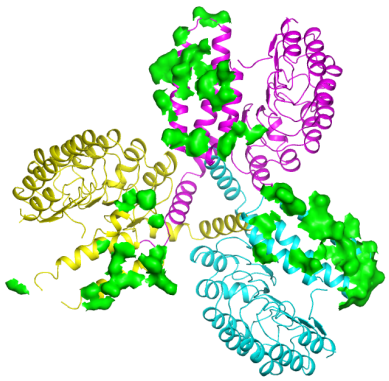

Figure S1. Multiple oligomeric forms of cNLRX1.
A. Gel filtration analysis of cNLRX1. The elution curves of the cNLRX1 and standards (thyroglobulin, 670 kDa; γ-globulin, 158 kDa; ovalbumin, 44 kDa; myoglobin, 17 kDa; vitamin B12, 1.4 kDa) as run over a Superdex 200 10/30 column are shown in red and blue lines, respectively. The purified recombinant cNLRX1 protein was eluted at two major peaks (monomer and hexamer) and one minor peak (dimer). **B**. Analytical ultracentrifugation analysis of cNLRX1. Sedimentation velocity profile (C(s) distribution

plot) is displayed and three peaks are resolved as forms of cNLRX1 monomer, dimer and hexamer in a concentration of 1 mg/ml. **C.** The non-crystallographic 3-fold rotational axis of the cNLRX1 trimer observed in the crystal. The unit cell is represented in black lines with corresponding axes and each monomer is represented in different colors. **Left**, Rotational angles between subunits are displayed and slightly deviate from being a perfect 3-fold (360°/3=120°) in the crystal. **Right**, The pseudo 3-fold axis (blue line) of the cNLRX1 trimer is tilted by ~2.5° from the crystallographic x-axis. **D**. Overlay of the three cNLRX1 subunits in the crystal ASU. Each subunit of cNLRX1 structure (subunit A, red; subunit B, cyan; subunit C, yellow) was superposed using Cα atoms of the LRRM domain. R.m.s.d.'s were calculated between equivalent Cα atoms for designated regions [all (residues 667-970); LRRNT (667-696); LRRM (697-901) and LRRCT (906-970)]. The individual LRRNT and LRRM domains are almost identical between subunits with r.m.s.d.'s of 0.1 Å. The $LRRCT^{C}$ domain exhibits the most dissimilarity from $LRRCT^{A}$ and $LRRCT^{B}$, consistent with the poorer quality of the electron density for that subunit. **E**. Crystal symmetry contacts of cNLRX1 LRRCT. Three cNLRX1 subunits in the ASU are shown in magenta (subunit A), cyan (subunit B), and yellow (subunit C) ribbons. LRRCT residues that make crystal lattice contacts (distances between atoms ≤4Å) are highlighted in a green surface presentation (subunit A, 64 atoms; B, 83 atoms; C, 36 atoms). The paucity of lattice contacts for subunit C explains the poorer electron density and greater disorder for that subunit compared to subunits A and B.

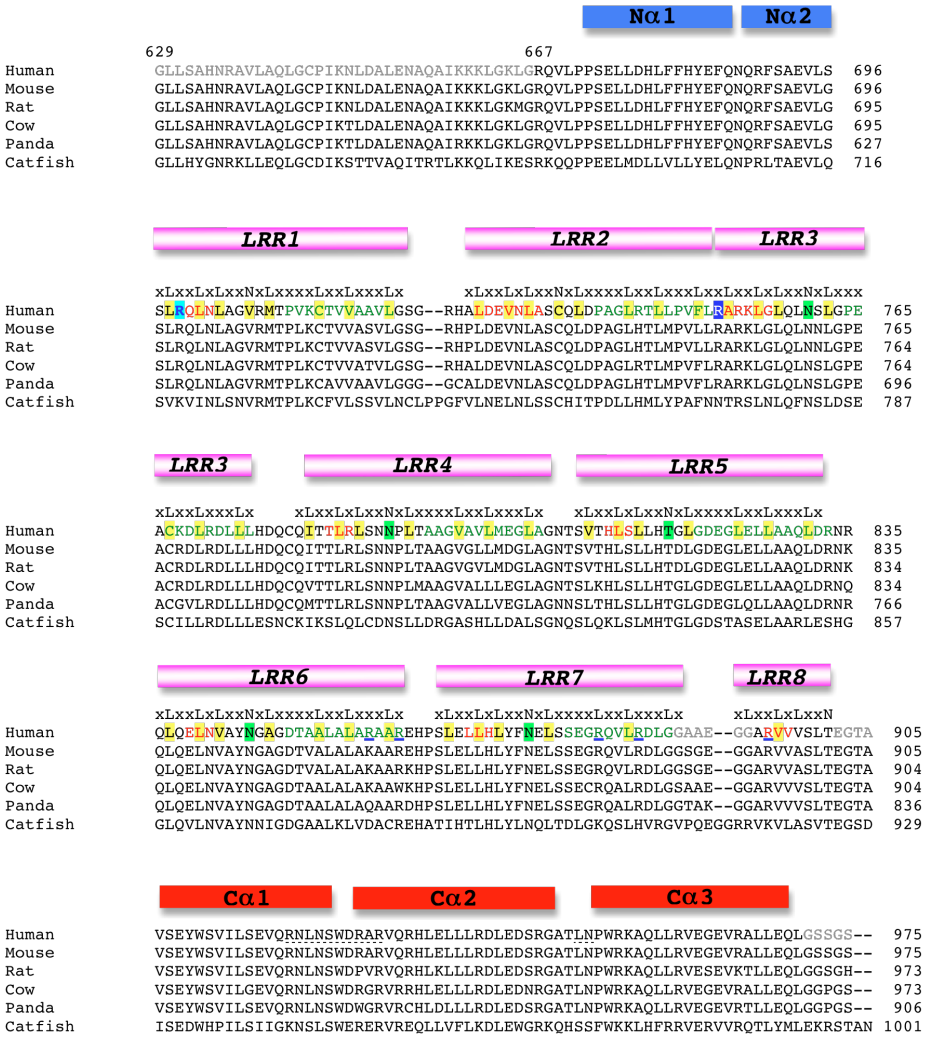

Figure S2. Primary sequence alignment of cNLRX1.
NLRX1 sequences in human, mouse, rat, cow, panda and catfish are aligned by *CLUSTALW2*. A schematic representation of the LRRNT α-helices, LRRM motifs, and LRRCT α-helices is shown in blue, magenta, and red rods, respectively, above the sequences. Consensus LRR sequences in the LRRM domain are shown above the sequence alignments, where 'x' denotes any amino-acid residue. Within the LRRs, conserved structural residues are highlighted in a yellow (hydrophobic) or green background (polar). LRR residues forming β-strands and α-helices are colored red and green, respectively. Arg751 is highlighted on a blue background. Residues 629-666, 887-893, 902-905 and 971-975 could not be built in the structure due to disorder in the crystal and are colored light grey. Residues missing only in subunit C are shown in dashed underlines. Arginine residues at LRR6 and LRR7 that cap the C-terminal LRRs are underlined in blue. In addition, arginine residue at 699 (Figure 5) is colored in blue and highlighted in cyan.

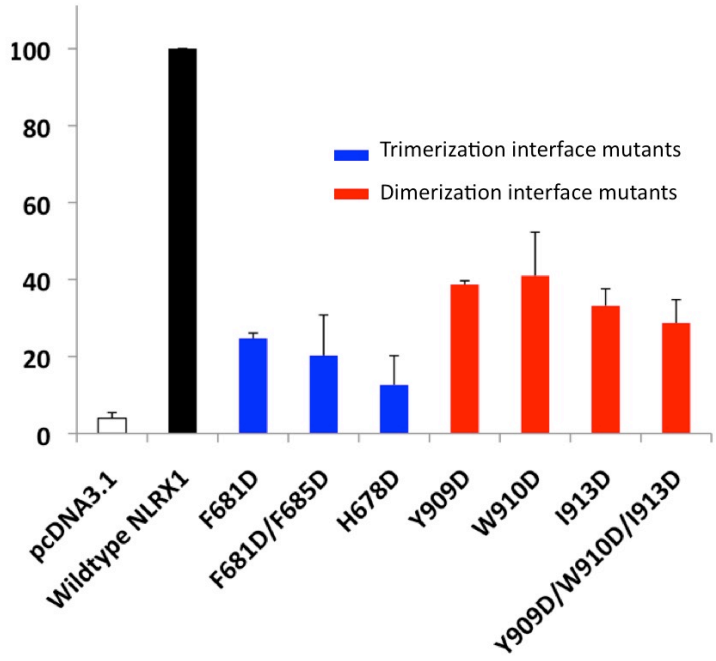

Figure S3. Decreased cellular ROS response of NLRX1 oligomerization-disruption mutants.

Wildtype and oligomerization-disruption mutant NLRX1 mammalian expression constructs were transiently transfected in HeLa cells for cellular ROS studies. ROS production was assessed after 3 hours of poly(I:C) stimulation and each value was normalized using that of the wildtype NLRX1 construct. Mutant constructs were labeled and colored accordingly.

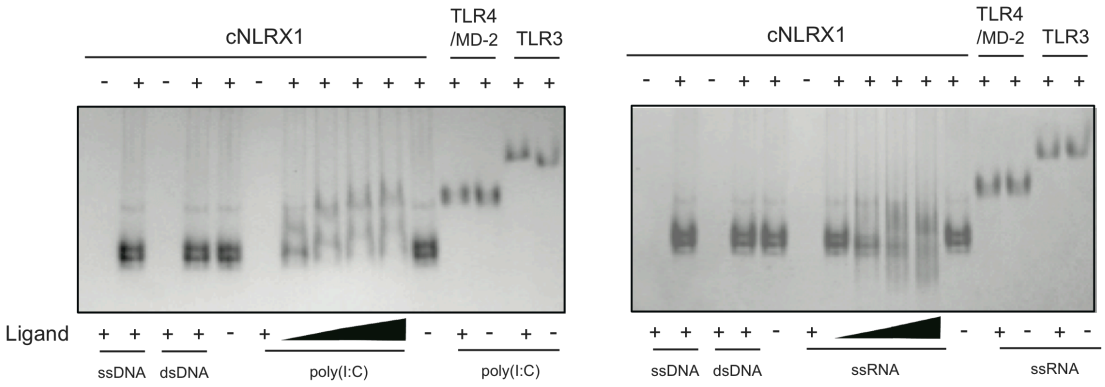

Figure S4. cNLRX1-RNA interaction.
cNLRX1 interaction with viral RNA mimic, poly(I:C) (left) and ssRNA (right) analyzed by native PAGE. The extracellular LRR domain of TLR4 in complex with MD-2 was included as a negative control. The extracellular LRR domain of TLR3 that binds only to dsRNA was included in the analysis as positive and negative controls for poly(I:C) and ssRNA binding, respectively.

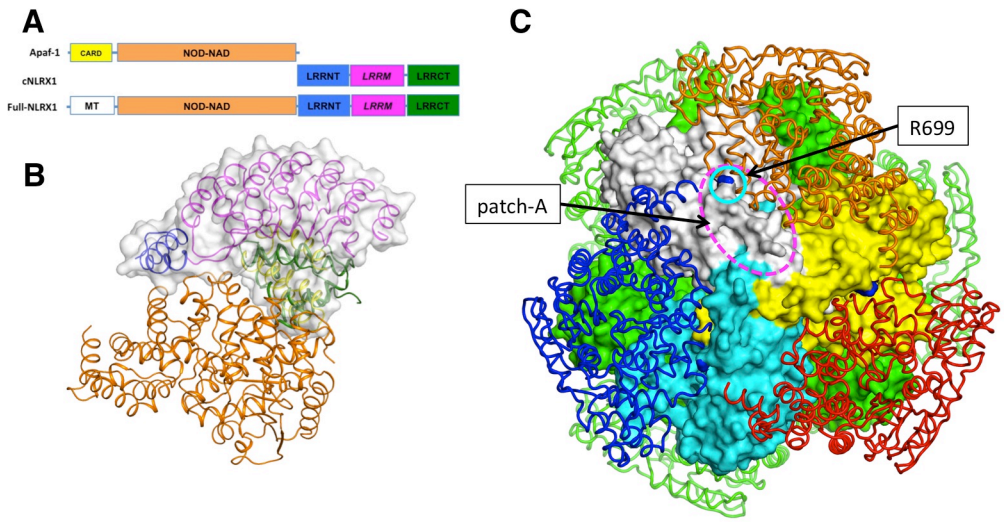

Figure S5. A homology model of full-length NLRX1 structure. Structure of full-length NLRX1 (Full-NLRX1) was modeled using Apaf-1 structure (PDB ID code 1z6t). **A**. The domain organization of Apaf-1, cNLRX1 and full-NLRX1. Each domain is distinguished by different colors. Apaf-1 contains CARD and NOD-NAD domains, which are absent in current cNLRX1 structure. **B**. NLRX1 does not contain any of putative effector binding domains. Assuming that NLRX1 LRRCT would be equivalent to the CARD of Apaf-1, CARD domain of Apaf-1 structure was superposed onto the LRRCT of the cNLRX1 monomer. cNLRX1 structure is shown in surface presentation. **C**, Model of full-NLRX1 hexamer. cNLRX1 is shown in surface representation (trimer-1, grey/cyan/yellow; trimer-2, green). A potential RNA binding patch-A that includes Arg699 is circled in magenta line. Arg699 residue is highlighted in blue surface presentation and circled in turquoise line. Model constructed from Apaf-1 structure is highlighted in coils (NOD-NAD domains of timer-1, orange/blue/red; those in trimer-2, light green). There was no observed steric crash between domains and subunits in the model.